Avionic Satellite Communication Terminal Requirements and Technology Maturity Analysis

Aparna P. T. Adithyababu, Federico Boulos, *Student Member, IEEE*, Stefano Caizzone

***Abstract*—Due to the increased demand for global connectivity, there has been a growing interest in the development and use of non-terrestrial networks (NTN) for applications (such as aeronautics) where terrestrial networks are not available or do not deliver satisfying performance. The use of newly deployed constellations in non-geostationary satellite orbits (NGSO) is getting much attention as it could potentially enable new performance levels in these applications, bridging the gaps of geostationary satellite orbit (GSO) systems. However, it has also lead to the need for more complex terminals, capable of continuously steering their beams towards the satellites. User terminals and their corresponding antennas become therefore crucial elements of the system. Its use in avionic systems has more features and constraints that are unique to the application. This paper focuses on the special constraints on the antenna terminal while taking into account an avionics satellite communication scenario and identifies potentialities and limitations of the use of NGSO systems as well as of the current technologies for airborne terminals.**

***Index Terms*—Airborne antenna, ARINC 791, ARINC 792, avionic terminal, NGSO, satellite communication.**

I. Introduction

NON-terrestrial networks (NTNs) have recently been receiving increased attention due to the growing need for global connectivity [1], [2]. NTNs can make use of spaceborne vehicles on low-earth orbit (LEO), medium-earth orbit (MEO), or geostationary earth orbit (GEO), as well as airborne vehicles such as unmanned aircraft systems (UAS), including high-altitude platforms (HAPS) [1]. The 3rd Generation Partnership Project (3GPP) [3], [4] sees NTNs as a viable solution to provide service continuity, ubiquity, and scalability to the 5th generation (5G) cellular networks. This suggests that NTNs could be used to increase coverage in remote regions and on mobile infrastructure, such as automobiles, aircraft, ships, and trains. The recent deployment of multiple LEO-based constellations, such as Starlink or Oneweb, has opened up new possibilities, with mobile broadband connectivity becoming more realistic worldwide. Aeronautics is one of the commercial sectors where ubiquitous communication via NTNs is particularly appealing. Satellite communication terminals are already available on commercial aircrafts, but they are often connected to geo-stationary orbit (GSO) systems, limiting the achievable bandwidth and causing geometry-induced latency problems. Due to the aircraft movement, satellite communication terminals for avionics need beam steering terminal antennas even when connected to GSO satellites. This requirement becomes considerably challenging if non-geo-stationary orbit (NGSO) systems are to be targeted, due to the necessity to continuously connect to (multiple) satellites in fast-moving directions. As a matter of fact, with respect to the Earth, the satellites in GEO are stationary and they orbit at an altitude of around 35786 km [3]. However, satellites in MEO (7000-25000 km) and LEO (300-1500 km), collectively known as NGSO, are moving relative to the Earth, necessitating a terminal characteristic of effective tracking to keep up with the satellite movement. For instance, the average speed of LEO satellites can be calculated as roughly 7.4 km/s [5] in reference to a fixed point on Earth, and hence appear to the terminal as rising and setting in less than 15 min [6]. Due to the high technological and commercial requirements, airborne terminals are currently among the most crucial system components, and numerous companies have committed to the endeavour of developing advanced next-generation avionic terminals in the recent years, aiming at fully exploiting the new possibilities given by the integration of GEO and LEO constellations.

The increasing demand for in-flight connectivity (IFC) by passengers is one of the main drivers for the deployment of broadband satellite communication in the avionics sector. The features and design of an avionic terminal differ from those of fixed terminals (or even from mobile terminals for different applications) due to unique constraints and requirements such as high (aircraft) speed and high dynamics (e.g., in banking turns), as well as the need for high aggregated throughput (due to the multiplicity of users/passengers connected to the same satcom terminal). The paper will investigate these peculiarities and identify the relevant challenges in the terminal design. Finally, an assessment of the technological maturity and compliance of the current commercially available systems with these requirements will be performed. Focus will be placed to systems operating in Ku (DL: 10.7-12.75 GHz, UL: 12.75-13.25 GHz, 14.0-14.5 GHz) [7] and Ka (DL: 17.7-20.2 GHz, UL: 27.5-30.0 GHz) bands [8], [9].

The paper is structured as follows: Sec. II. talks about the avionic specific requirements for the antenna terminal detailing about the ARINC 791 [10], [11] and 792 standards [12]. Sec. III. talks further about the technical requirements for avionics specific terminal. Thereafter, a detailed link budget was performed considering an aircraft terminal scenario using LEO and GEO connectivity and the results are discussed in Sec. IV. Finally, the adequacy of the present terminal antenna technology was compared in Sec. V.

A. P. T. Adithyababu, F. Boulos and S. Caizzone are with the Institute of Communications and Navigation, German Aerospace Center (DLR), Wessling, Germany (e-mail: Aparna.Parakkalthachappillyadithyababu@dlr.de, Federico.Boulos@dlr.de, Stefano.Caizzone@dlr.de)

II. Avionic Specific Regulatory Constraints for The Antenna Terminal

The aircraft's satellite communication terminal must adhere to strict technical regulations in both mechanical and electrical terms, which are detailed in ARINC standard documents 791 [10], [11] and 792 [12]. This section discusses the most relevant regulatory constraints of ARINC standard for Mark I and II aviation satellite communication systems.

A. ARINC Standards

The ARINC standards 791 and 792 outline the desirable properties of Ka band and Ku band satellite communication systems in particular, to be installed on all types of commercial air transport aircrafts. The purpose of this standard is to offer recommendations on the system interfaces, form, fit, and functionality.

1) ARINC 791: The aircraft earth station (AES), consists of an outside antenna equipment (OAE), a Ku/Ka band radio frequency unit (KRFU), a Ku/Ka band aircraft networking data unit (KANDU) (collectively known as an antenna subsystem), and modem/manager (ModMan). The ModMan is further connected to airplane personality module (APM). Fig. 1 shows a simplified version (details about the components in each blocks are not included) of the baseline functional block diagram of the AES with the aforementioned blocks along with the connections and bulkhead interfaces (BI). The general block diagram in Fig. 1 applies to a fuselage-mounted antenna (FMA). Furthermore, ARINC 791 [10] provides nine other possible alternate configurations with minor structural differences from the baseline.

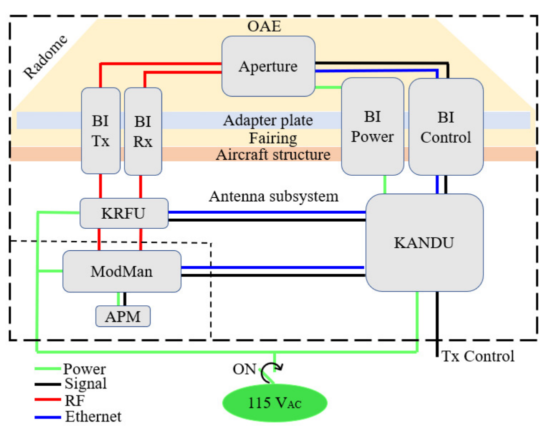

Fig. 1. Simplified baseline functional block diagram of ARINC 791 AES.

The ModMan, KRFU, and KANDU each receive 115 V AC power from the aircraft power supply. The rest of the AES is then powered by KANDU, whose total power usage should not exceed 500 W. The antenna aperture, Low Noise Amplifier (LNA), polarization control unit, positioner, adaptor plate, radome, and fairing are all part of the OAE. In the case of a tail-mounted antenna (TMA) (usually in regional aircrafts), the KRFU is placed in the OAE. The TMA may use a horn antenna or a circular parabolic reflector and it does not require the use of an adapter plate or a fairing.

According to the lug (7 lugs) arrangements, ARINC 791 fitting layout for FMA extends up to a total footprint of width (perpendicular to flight direction) 76.2 cm and length (along flight direction) 190.5 cm [10]. Since these mentioned values specify the extend of the lugs, the actual dimension of the adapter plate can be slightly larger. For instance, the ARINC 791 compliant Flightgear™ adapter plate in [13], specifies a width of 108.5 cm and length 265.7 cm. It moreover specifies a maximum of antenna swept diameter of 95.25 cm and a swept height of 24.4 cm. For a TMA, the highest allowable swept volume height and swept diameter are approximately 34.5 cm and 30.5 cm [10], respectively. Since ARINC 791 supports, often partly mechanically steerable, the OAE should be spacious enough to enable rotation in a low profile enclosure. Terminals adhering to this standard (referred to as ”First generation terminals”) are already available on the market and used in commercial aviation aircraft.

2) ARINC 792: A second generation (Mark II) aviation satellite communication system for all types of aircraft is described in ARINC 792 [12]. The focus here is on specifications for flat panel antennas that have integrated beam steering and RF circuits in order to support the expanding NGSO satellite networks. The OAE, Ku/Ka-band power supply unit (KPSU), and ModMan are listed in the standard [12] as the main units of the ARINC 792 AES. The ModMan and KPSU works in 115 V AC power where the KPSU may use three-phase or single-phase power. According to [12], the KPSU that powers the OAE has a power consumption limit of 2200 W with a three-phased power supply and 500 W with a single-phase power supply. Compared to ARINC 791, ARINC 792 OAE consists of additional components such as RF high power amplifier , up convertors, down convertors, antenna control, and monitoring.

Comparatively, ARINC 792 features simpler wiring and fittings and the lug (6 lugs) layout has a footprint width of 87.8 cm and a length of 127 cm (shortest layout) to 226.1 cm (longest layout) [12]. An antenna aperture scalable up to 106.68 cm [14] can be accommodated in ARINC 792 system.

B. Interference Limitation

It is of paramount importance to strictly control the radiation of transmitting terminals and avoid possible interferences to other systems, onboard the aircraft or on satellites. To ensure it, avionic terminals must meet two functional requirements: radiation blockage capabilities based on aircraft geometry and radiation limitations according to the regulatory masks.

1) Radiation Blockage: When the satellite is at a high scan angle from the broadside of the terminal, beam steering towards the aircraft fuselage may result in scattering and reflected radiation. Apart from the main lobe, the side lobe could also be scattered by the aircraft structures such as VHF blades and the vertical stabilizer [11]. This energy can potentially become an interference if it reaches unwanted satellites and this must be strictly avoided. The antenna must be able to mute the transmitter in such circumstances. This can be carried out using a blockage table, which serves as a look-up table and takes into account the aircraft's geometry and the location of the terminal. Whenever the beam is steered to a new direction, the table (usually stored in the ModMan) can be utilized to control the mute operation. This is accomplished through the Tx control signal shown in Fig. 1.

2) Regulatory Masks: Standardisation bodies propose various reference radiation masks for earth stations operating in different frequencies to limit the emission of the terminal radiation and reduce the interference to other satellites in the GSO arc. For instance, in the plane tangent to the GSO arc, the co-polarization gain of any earth station antenna transmitting to a GSO satellite in the frequency range 24.75-25.25 GHz or 27.5-30 GHz should not exceed the following limits [15]:

$$\text{Gain (dBi)} = \begin{cases} 19 - 25 log\phi, & \text{for } 2^\circ \leq \phi \leq 7^\circ \\ 8, & \text{for } 7^\circ < \phi \leq 9.2^\circ \\ 32 - 25 log\phi, & \text{for } 9.2^\circ < \phi \leq 19.1^\circ \\ 0, & \text{for } 19.1^\circ < \phi \leq 180^\circ \end{cases} \tag{1}$$

where ϕ is the angle from the bore-sight (direction of the main lobe) of the terminal beam, when the beam is pointing to the target satellite. The numerical gain values in (1) can be depicted graphically with respect to the mentioned angular limits as shown in Fig. 2.

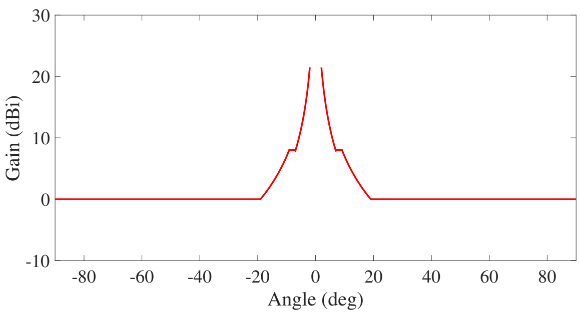

Fig. 2. Regulatory mask for co-polarization gain of an earth station transmitting antenna.

To avoid interfering with other satellites, the terminal is only permitted to alter its radiated power up to a particular threshold. This radiation power constraint is represented by the power spectral density (PSD), which is normally expressed as a ratio of effective isotropic radiated power (EIRP) to bandwidth, with respect to the angular limits. For instance, in the plane tangent to the GSO arc, the off-axis PSD envelope of the co-polarized transmission from earth stations operating in the Ka band is given by [16],

$$\text{PSD(dBW/MHz)} = \begin{cases} 32 - 25 log\phi, & \text{for } 2^\circ \leq \phi \leq 7^\circ \\ 11.5, & \text{for } 7^\circ < \phi \leq 9.2^\circ \\ 35.5 - 25 log\phi, & \text{for } 9.2^\circ < \phi \leq 19.1^\circ \\ 3.5, & \text{for } 19.1^\circ < \phi \leq 180^\circ \end{cases} \tag{2}$$

where ϕ is the angle from the bore-sight (direction of the main lobe) of the terminal beam, when the beam is pointing to the target satellite. The angular limits shows that the PSD is strictly controlled from 2° away from the target satellite. PSD control operations at the terminal should ensure that the regulatory mask is not breached and no interference is exerted on nearby satellites. The ModMan analyses antenna radiation performance, adjusts the transmit power by altering the power provided to the antenna system, and determines the appropriate modulation and coding to ensure PSD mask compliance [11].

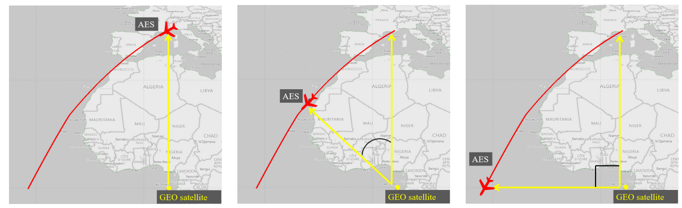

(a) Skew angle 0°. (b) Skew angle 45°. (c) Skew angle 90°.

Fig. 3. STK 2D view showing skew angle variation during aircraft flight.

The skew angle is an important factor influencing the PSD control in aircraft satcom terminals. Assuming a flat Earth, the skew angle is estimated by drawing a radial from the point on the equator exactly beneath the target satellite to the ARINC 791 satcom system [11]. The skew angle concept is illustrated in Fig. 3 using a 2D view from the Ansys System Tool Kit [6], which shows the aircraft and satellite positions at three different time instances, resulting in skew angles of 0°, 45°, and 90°. The radiation pattern from the AES as seen at the target GSO satellite during the three instances in Fig. 3 was examined to demonstrate the effect of the skew angle. For example, consider a circular parabolic reflector antenna as the AES terminal that can be mechanically steered to the target GSO satellite. The pattern observed at the satellite is circularly symmetric (equal beam width in azimuth and elevation) irrespective of the skew angle (irrespective of AES position) as shown in Fig. 4. Therefore a single value (e.g., 1 dB) can be given as a power back off whenever the radiation is interfering the neighbour satellites.

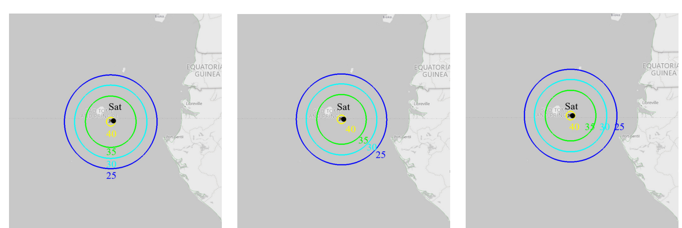

(a) Skew angle 0°. (b) Skew angle 45°. (c) Skew angle 90°.

Fig. 4. STK view showing 2D gain contours of AES's symmetric antenna radiation pattern as seen at the GSO satellite.

However, as illustrated in Fig. 5, a uniformly illuminated rectangular aperture antenna with an asymmetric radiation pattern has different beam width in azimuth and elevation. According to [11], the low profile antennas on aircraft with asymmetric patterns can have a beam width of about 7° in elevation and about 0.5° in azimuth. The GSO satellites are around 2° [11] apart when viewed from the Earth. In such cases, a skew angle of 0° is the most favourable value, while 90° is the least favourable. For example, in Fig. 5a, when the

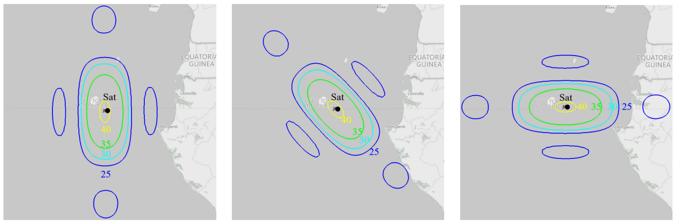

(a) Skew angle 0°. (b) Skew angle 45°. (c) Skew angle 90°.

Fig. 5. STK view showing 2D gain contours of AES's asymmetric antenna radiation pattern as seen at the GSO satellite.

skew angle is 0°, the narrow azimuth beam is aligned along the GSO arc, resulting in less interference with neighbouring satellites, whereas in Fig. 5c, when the skew angle is increased to 90°, the broader elevation beam is aligned along the GSO arc, potentially interfering with nearby satellites. Therefore, in such terminals with asymmetric antenna radiation patterns, the ModMan requires a table of PSD back off values (instead of a single value) to reduce the transmit power according to the monitored skew angle. In general, the broader the beam width along the GSO arc, the greater the interference and the lower the PSD available for transmission.

C. Data Rate

The target performance (for theoretical analysis) for aircraft connectivity using NTN has been set by 3GPP [3] at 360 Mbps in downlink (DL) and 180 Mbps in uplink (UL), taking into account an aircraft travelling at 1000 km/hr with an average of 120 users. This indicates that each end user will receive 15 Mbps in DL and 7.5 Mbps in UL.

III. Avionic Specific Technical Constraints for the Antenna Terminal

The regulatory constraints described in Sec. II influence the achievable performance and determine the technological constraints for the avionic terminal.

A. Available Gain

The regulations on maximum size directly impact the maximum achievable gain [5] of the airborne terminal, therefore impacting the EIRP and gain over temperature (G/T) parameters (see next section). The dimensions allowed for Flightgear™ ARINC 791 and 792 Ka, Ku, Ka/Ku universal installation adapters (fuselage mounted), for instance, are up to 95.25 cm (swept diameter) [17] and 106.68 cm (aperture size) [14], respectively. The maximum achievable gain with the given dimensions is shown in Table I. The estimate was performed at the lowest edge of the appropriate frequency band (Ka), taking into account a uniformly illuminated rectangular antenna aperture of ideal efficiency 100%.

B. Impact of Scan Angle

The maximum achievable gain, as computed in Table I, is usually obtained at broadside (direction perpendicular to antenna aperture). However, airborne terminals will need to steer their beam at a scan angle $\theta°$ with respect to the broadside vector to follow the satellite position. Since the entire aperture of a mechanically steered antenna can be rotated in the direction of the satellite, it can deliver maximum gain in all pointing directions. The gain of flat panel antennas, on the other hand, drops [18], [19] when the beam is steered away from the broadside, and the reduction is faster at greater angles [18]. For instance, Fig. 6 shows the mentioned reduction of the DL gain for the ARINC 792 terminal from the maximum value calculated in Table I.

TABLE I
Maximum achievable gain

Max aperture (cm)	Tx (UL) Gain (@27.5 GHz)	Rx (DL) Gain (@17.7 GHz)
ARINC 791: 95.25	46.80 dBi	42.98 dBi
ARINC 792: 106.68	47.79 dBi	43.96 dBi

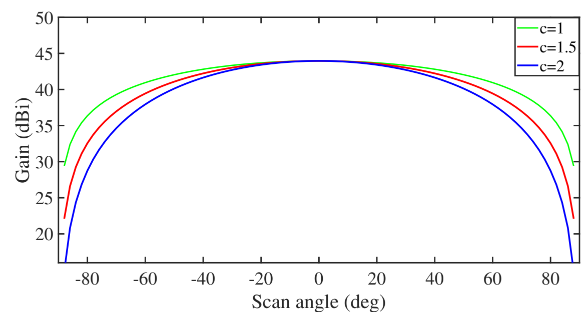

Fig. 6. Variation in gain with scan angle for distinct cosine roll-off (c) values.

As shown in Fig. 6, the cosine roll-off (an antenna coefficient for gain reduction) is a common method for evaluating this gain reduction based on the scan angle. Therefore, the achievable gain at high steering angles will vary depending on the levels of cosine roll-off attained by various terminal technologies. In any case, since the gain at high scan angles is lower, NGSO constellations can be favourable to such antennas by lowering the required scan angle for connectivity.

C. Handovers and Multibeam

During the journey, the aircraft crosses several satellite beams and a handover happens when the network requires the system terminal to switch from one beam to another. If both beams are on the same satellite vehicle (SV), the handover is referred to as intra-SV, whereas if the beams are on separate satellites, the handover is referred to as inter-SV [12]. Additional to re-tuning the receiver chain to a different radio frequency channel, the terminal's polarization might as well be altered for intra-SV handover. For an inter-SV handover, antenna's pointing angle must also be adjusted.

For the spot beams on high throughput satellites of about 2° beam width, a handover may take place once every 90 min [12]. Wide beam handovers may only occur once per flight and will be an intra-SV handover. Given that the satellites are rising and setting more quickly relative to the airborne terminal, NGSO handovers may occur more frequently. The number of beams per satellite and the constellation orbit both affect the frequency of NGSO handovers. Intra-SV and inter-SV handovers could occur as frequently as every 11 s and 3 min, respectively, as stated in [12]. As a result, the antenna terminal should be designed so that the beam steering operation requires less than 1 ms [12].

More than one usable beam may be generated at the terminal in order to keep up with concepts for hybrid LEO/GEO operations and to provide capabilities such as make-before-break handovers [12]. The terminal antenna must be capable of producing several simultaneous beams from a common aperture, each having its own pointing angle, centre frequency, and polarization state. Each beam should ideally utilize the complete aperture, maintain its full gain and power, and avoid producing out-of-band spurious emissions.

D. Environmental Challenges

Flying at a high altitude of up to around 15 km, an aircraft terminal is subject to harsh environmental conditions (temperature and humidity), which presents a challenge to the antenna and the radome. Ambient temperature can reach as low as $-78°$ C [10]. Due to the temperature difference between the inner surface of the radome and the airflow, heat is transferred through it. Additionally, local heating is produced when air strikes the radome's leading edge (ram-air effect which can rise the ambient temperature by $40°$ C [10]). This is accompanied by the heat from the equipment that is positioned beneath the radome, the underlying aircraft surface, and solar radiation. As a result, the ambient temperature inside the radome can increase up to $55°$ C [10]. When designing thermal management, these tough conditions must be taken into account to limit overheating effects.

IV. Link Budget Analysis

A link budget analysis was carried out according to the procedure mentioned in [1] and [19] to examine the achievable performance of an antenna terminal under the avionic-specific limitations described in Sec. II and III. In particular, the purpose was to assess the differences in achievable performance between GSO and NGSO systems, as well as quantify the additional complexity in NGSO scenarios. The link performance was studied by estimating the figures of merit (FoM) for forward DL and return UL, namely, carrier-to-noise ratio (C/N) and throughput (*Th*) using [1]

$$\begin{aligned} \text{C/N (dB)} = \text{EIRP (dBW)} - \text{BW (dBHz)} - \text{FSPL (dB)} \\ + \text{G/T (dB/K)} - k\text{(dBJ/K)} \end{aligned} \tag{3}$$

$$\textit{Th} \text{ (Mbps)} = \text{SE (bps/Hz)} \times \text{BW (dBHz)} \tag{4}$$

where EIRP is the effective isotropic radiated power of the transmitter, BW is the carrier bandwidth, FSPL is the free space path loss in the transmission medium, G/T is the gain to system temperature ratio of the receiver, and k is the Boltzmann's constant (-228.6 dBJ/K). The spectral efficiency (SE) was calculated using the Shannon's limit [1]. Table II lists the assumptions made regarding the terminal and satellite to implement the computations. The assumptions are detailed in the Appendix.

TABLE II
Assumptions for link budget analysis

Parameters	Values
User terminal	
Diagonal dimension (cm)	106.68 [12]
Input power (W)	20 [20]
System temperature (dBK)	24.3 [5], [6], [19]
Cosine roll-off	1
Efficiency (%)	75% [5]
Satellite	
EIRP (dBW)	GEO 54.0 [21]
	LEO 39.4 [22]
G/T (dB/K)	GEO 7.0 [21]
	LEO 9.8 [22]

TABLE III
Calculated terminal antenna parameters

Parameters	$\theta = 0°$
G/T (dB/K) @ 17.7 GHz	18.3
EIRP (dBW) @ 27.5 GHz	59.5

TABLE IV
Link budget: Terminal on aircraft

FoM	GEO $\theta = 0°$	LEO $\theta = 0°$
C/N (dB)	DL 12.4	34.28
	UL 5.84	45.09
SE (bps/Hz)	DL 4.21	11.38
	UL 2.27	14.97
Th (Mbps)	DL 421	1138
	UL 113	748

The terminal parameters such as G/T and EIRP were calculated at terminal's broadside (scan angle $\theta = 0°$) and are displayed in Table III. The estimated FoM, which were calculated assuming the satellite to be at the terminal's broadside, are shown in Table IV. It is worth highlighting that scenario or implementation dependent terms (such as rain fading effect, atmospheric losses, interference) have been neglected for simplicity. Therefore, the results displayed in Table III and IV can be considered as upper bound (theoretical) performance. Although the results are theoretical, it is important to point out that a GEO satellite link makes it difficult to successfully close the link due to the comparatively low C/N. Unlike LEO satellites, GEO satellite-user communication links experience a comparatively high level of FSPL [1] due to their large distance from the Earth, lowering the C/N according to (3). Also, in reality, satellites may not be accessible from the terminal's broadside, necessitating beam steering. As stated in Sec. III, when the scan angle widens, the gain decreases and the FSPL increases [1], lowering the C/N (both in DL and UL) according to (3). For instance, Fig. 7 shows the mentioned effect of scan angle on the downlink C/N. This eventually causes a drop in throughput as well according to (3-4).

Ansys STK [6] was used to simulate the link performance in a more realistic scenario, where the afore-mentioned terminal

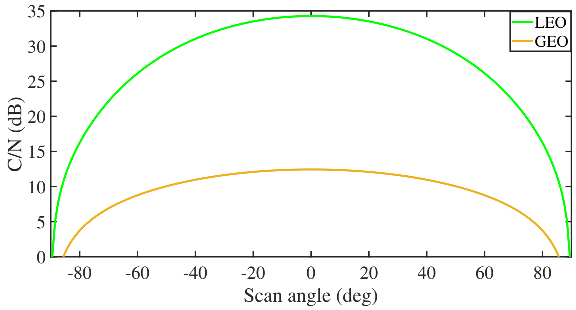

Fig. 7. DL C/N variation with scan angle for LEO and GEO scenarios.

was considered to be installed on the fuselage of an aircraft. Two separate flight routes F1 and F2 were considered for the analysis. The necessary information, such as the aircraft type, flight waypoints, cruising altitude, and speed, were obtained using the tracking logs of flights UAE52 and DLH500 [23]. The analysis was simplified by focusing just on the cruising phase. Table V displays the coordinates of the start and end of the cruising period assigned to the aircraft in STK, cruising duration, and aircraft type. Note that the flight route F1 is in the northern hemisphere, while flight in route F2 is transatlantic and eventually crosses the equator to travel to the southern hemisphere.

TABLE V
DETAILS ON FLIGHT ROUTES F1 AND F2

Route	Cruise Start (Lat, Long)	Cruise Stop (Lat, Long)	Duration (hr)	Aircraft Type
F1	$47.6°, 15.5°$	$27.2°, 53.1°$	4.3	A380-800
F2	$46.1°, 10.6°$	-21.9°, -42.2°	10.1	A350-900

In order to carry out the required analysis, necessary GEO and LEO satellites should be considered. For the NGSO case, the Starlink LEO constellation, which consists of 4236 satellites [24] orbiting on various orbital planes, is incorporated into the scenario. The Starlink satellites' EIRP and G/T in STK were assumed to be the same as prior assumptions in Table II. Fig. 8a displays the flight routes F1, F2 and the Starlink LEO constellation. Eutelsat 7B [21] was considered for the GEO case analysis and is depicted in Fig. 8b. The EIRP and G/T for the GEO satellite was taken from Table II.

During the aircraft's flight, the GEO satellite is stationary relative to the Earth whereas LEO satellites are in motion. Therefore, over the entire journey, the LEO satellites performs multiple number of passes over the aircraft terminal, resulting in multiple access instances. For instance, Fig. 9 shows the downlink C/N that the terminal encountered as a result of three passes by a single Starlink satellite, in route F2. As the aircraft terminal and satellite get closer and farther apart, the C/N curve will rise and fall, as was shown earlier in Fig. 7.

The terminal on the aircraft was considered to operate with a field-of-view (FoV) of 90° (from the broadside of the terminal). Considering the entire Starlink LEO constellation for flight routes F1 and F2, a total of 7304 and 12738 satellite access instances (including multiple passes by same satellite)

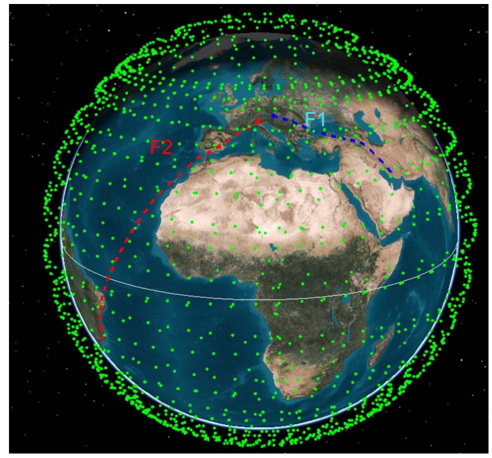

(a) Starlink constellation denoted by green markers, F1 and F2 denoted by blue and red dotted lines, respectively.

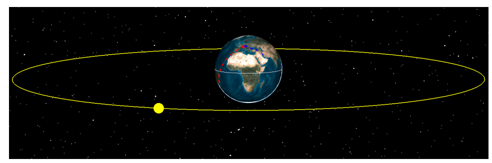

(b) Eutelsat 7B satellite denoted by yellow marker.

Fig. 8. STK view from (a) LEO and (b) GEO scenarios.

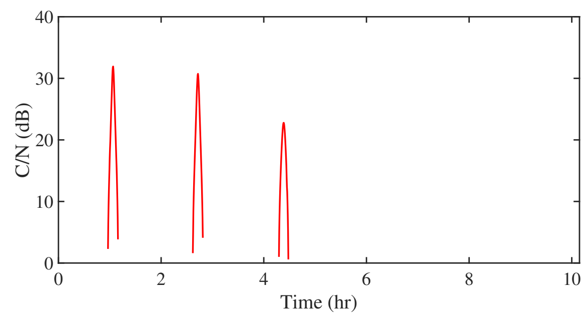

Fig. 9. Downlink C/N with a single Starlink satellite in F2.

were recorded, respectively. The resulting C/N curves due to the multiple passes by different satellites during the journey in route F2 is shown in Fig. 10. Similarly, C/N plots for flight routes F1 and F2 in the GEO scenario were generated and are shown in Fig. 11a and 11b, respectively. Since the flight route F1 is relatively short and positioned in the northern hemisphere, there is minimal variance in the C/N in GEO scenario. The occasional peaks or discrepancies in the curve will be explained later. For F2, the GEO C/N curve initially displays a progressive rise, peaks when the aircraft crosses the equator (in close vicinity to GEO satellites), and then declines as the flight proceeds further towards the southern hemisphere.

The aircraft will occasionally ascend, descend, or makes turns along its flight path, for instance, as depicted in Fig. 12. The up and down movement of the aircraft wings during this phase can be represented by the bank or roll angle [25]. The pitch angle can be used to depict the up-and-down movement of the aircraft nose, while the yaw angle can be used to

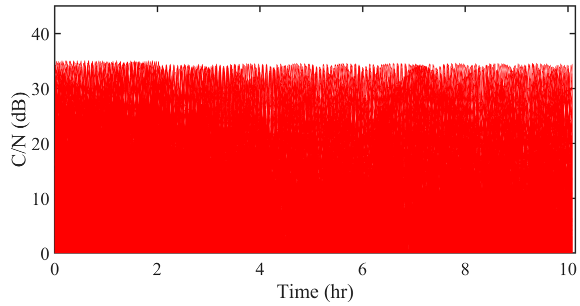

Fig. 10. Downlink C/N for LEO scenario for F2.

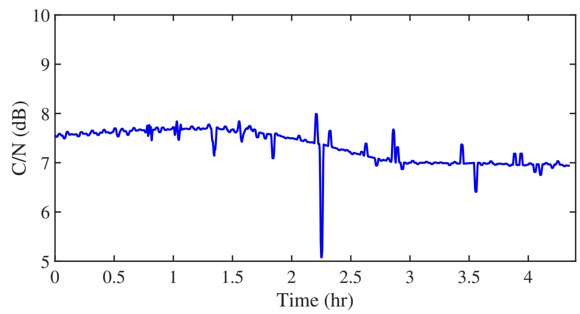

(a)

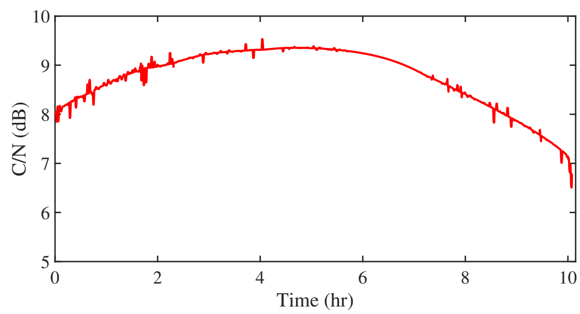

(b)

Fig. 11. Downlink C/N for GEO scenario for (a) F1 and (b) F2.

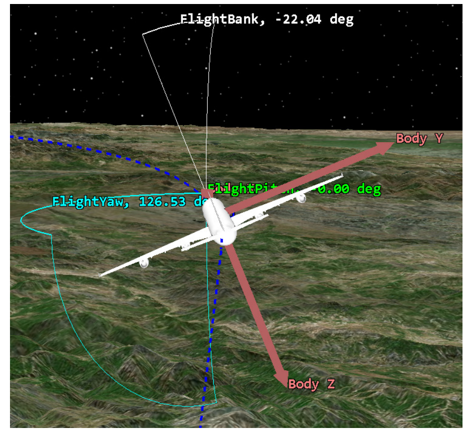

Fig. 12. STK view of the aircraft in F1 making a left turn.

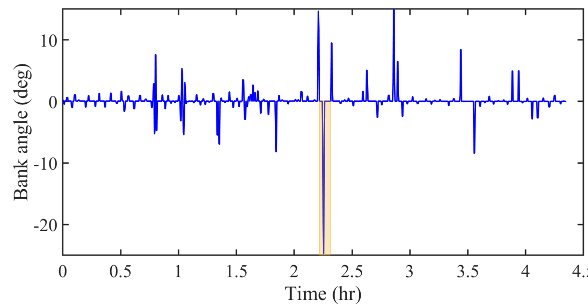

Fig. 13. Bank angles in F1 highlighting the banking instance in Fig. 12.

depict its left- and right-lateral movement [25]. In Fig. 12, the aircraft in F1 can be seen making a turn to the left along its route, resulting in a bank angle, pitch angle, and yaw angle of $-22.04°$, $0°$, and $126.53°$, respectively. The axes X (directed towards the nose of aircraft), Y (directed towards right wing), and Z (directed downwards, perpendicular to X and Y) represented in the figure are the body axes of the aircraft.

The aircraft's bank angles were plotted for the entire journey in F1 in Fig. 13 in order to comprehend the impact of aircraft manoeuvring on the resulting link performance. One of the banking events is highlighted in Fig. 13 (at around 2.25 hr of F1 journey) which corresponds to the aircraft banking in Fig. 12. The variations in the scan angle and downlink C/N that the terminal in route F1 experienced is depicted in Fig. 14a and Fig. 14b for the LEO and GEO scenarios, with the banking event being highlighted. Only one of the satellites in LEO constellation was chosen to provide a better view of the discrepancy in LEO scenario. The aforementioned remarks on Fig. 10 make it clear that the terminal observes a large number of satellites with the potential for connectivity in LEO case. However, the terminal must scan its beam in order to connect to the satellites successfully because of the relative motion between the aircraft and satellite. As shown earlier in Fig. 7, this leads to a variation in the resulting C/N. Being positioned on top of the aircraft, the terminal's FoV moves along with the aircraft during manoeuvring. As a result, when the aircraft banks, some satellites in the terminal's field of view gets closer or farther away, altering the required scan angle for connectivity. As a result, Fig. 14a and 14b show the corresponding effect on the C/N curve for LEO and GEO satellites. It is also important to note that the C/N fluctuations in the GEO scenario are more gradual than the sudden surge or fall in the LEO scenario. This occurs because LEO satellites move relative to the Earth, whereas GEO satellites remain stationary. Furthermore, there are certain limitations on the aircraft angles which may depend on the aircraft type, flight mode, flight configuration, etc. For instance, a maximum bank angle of $\pm 67°$ is permitted under "Normal law" in [26] and [27], for Airbus $A380-800$ and Airbus $A350-900$ aircrafts in clean configuration, respectively.

Along with the C/N values, the scan angles to the satellites for both flight routes (F1, F2) for the GEO and LEO scenario were recorded at a time interval of 20 s, taking into account the aircraft's banking events as well. The majority of LEO satellites were visible for both aircraft routes at an angle of $80°$ to $90°$ from the terminal's broadside, according to Fig.

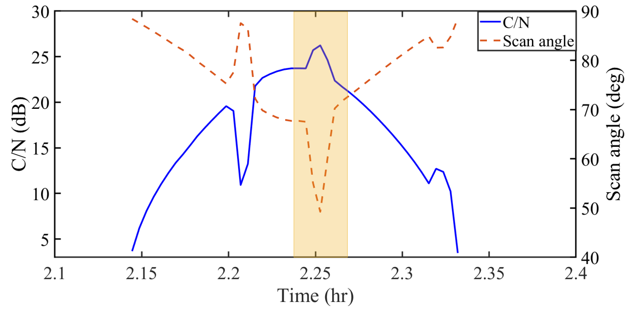

(a)

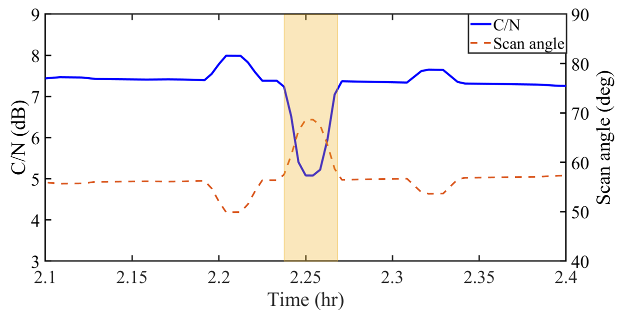

(b)

Fig. 14. Variation in scan angle and DL C/N corresponding to Fig. 12 for (a) LEO scenario and (b) GEO scenario.

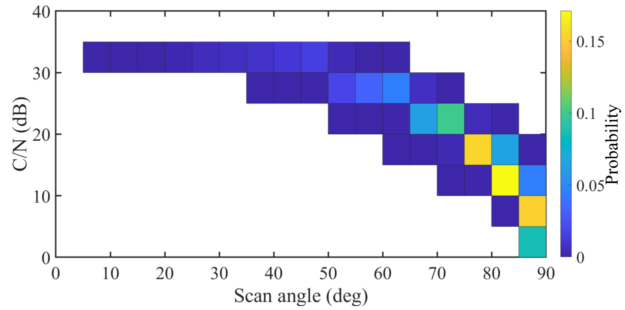

(a)

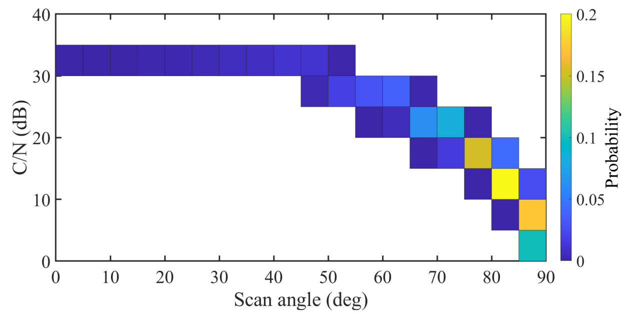

(b)

Fig. 15. LEO access probability at observed scan angle with corresponding C/N for (a) F1 and (b) F2.

15. However, a better C/N is obtained when the satellites are near to the broadside of the terminal. In the GEO scenario, the terminal along route F1 is in the northern hemisphere, whereas the terminal in F2 travels into close proximity to GEO as it crosses the equator. Therefore, most of the accesses for route F1 appear in Fig. 16a at a scan angle between $55°$ and $60°$, whereas most of the accesses for route F2 appear in Fig. 16b at a relatively smaller scan angle between $40°$ and $45°$. Furthermore, when the LEO and GEO scenarios for both routes are compared, it is clear that LEO satellites are visible at a lower scan angle than GEO satellites.

V. Adequacy of Present Technology

Several technologies have been investigated in the last few years to provide a reliable and robust user terminal for satellite communications, both for aeronautical and non-aeronautical applications. Some of them matured sufficiently to allow commercial products to appear on the market. Multiple terminal systems implementing various technologies are available on the market in avionics; they will be compared in this section in terms of the achievable performance with the simple link budget analysis shown in the previous section, using publicly available antenna performance parameters of the terminals. In Table VI the satcom terminals that are currently commercially available (to the best of authors' knowledge) are listed and assessed with respect to the multiple avionic features previously addressed in Sec. II and III. For each of the terminals given, the frequency band of operation, scan angle extend, terminal size, ARINC size compliance, G/T and EIRP values at the broadside are specified. Note that the dimensions listed in the table corresponds to the entire customer terminal. The notes TX and RX emphasize the dimension related to the antenna alone. The different terminals can be classified in macro-areas based on their underlying technology as:

- Classical Phased Array: Represented by Viasat, Extreme Waves, Alcan, Ball Aerospace, JetTalk, Gilat and XPhased.
- Holographic Antenna: Represented by Kymeta.
- Lens Antenna: Represented by All.Space
- Variable Inclination Continuous Transverse Stubs (VICTS): Represented by ThinKom.
- Mechanical Antenna: Represented by Hughes.

The reader is invited to consult [42][1] for further details on antenna array technologies. It is worth to be mentioned that not all of the presented technologies in Table VI are designed for specific avionics purposes but they will be equally presented for the purpose of completeness of the analysis. Table VI shows for instance substantial differences in the scan angles from a minimum of $55°$ (from bore-sight direction) to a maximum of $80°$ in the case of flat arrays. A full coverage (e.g., $0°$ to $90°$ in elevation and $0°$ to $360°$ in azimuth) is achieved only by using a mechanical antenna array at the cost of a moving platform. Moreover, it can be noticed that the non-avionics terminal exhibits a scan angle up to $75°$ whereas the scan angle goes up to $90°$ for the avionics terminal. This wide FoV will aid the terminal in the event of the previously described banking turns. There are also commercial terminals from All.Space, Starlink, Amazon Kuiper, QEST, GreenerWaves, C-COM, etc. However, very little to no public

[1]Keep just if we receive review in the meantime otherwise to remove.

TABLE VI
COMPARISON OF COMMERCIAL SATCOM USER TERMINAL ANTENNAS

Antenna	Frequency Band	Scan Angle (deg)	Terminal Size (cm)	ARINC Size Compliance	G/T (dB/K)	EIRP (dBW)
Avionics Terminals						
ThinKom [28], [29]	Ku	82.5	187.96 × 88.9 × 10.67	791, 792	18.5	57
	Ka		142.24 × 81.28 × 9.4			55.5
Viasat [30]	Ka	70	105 × 55 × 7	791, 792	15	58
Ball Aerospace [31] [32]	Ku	80	48.26 × 48.26 (TX)* 58.42 × 58.42 (RX)*	791, 792	12.5	53.6
	Ka		40.64 × 40.64 (TX)* 45.72 × 68.58 (RX)*	791, 792	15.8	53
JetTalk [33]	Ku	80	160 × 87 × 5.5	791, 792	14	49
	Ka				17	
Hughes [34]	Ku	90	95.7 × 95.7 × 23.8	791	11.6	43
	Ka				15.4	48
Gilat [35]	Ka	70	40.1 × 58.2 × 11.16 (TX)* 44.7 × 58.2 × 9.93 (RX)*	791, 792	11.4	50.2
Non-avionics Terminals						
Extreme Waves [36]	Ku	70 – 75	n.a. (1024 elements)	-	11.2	47 – 48
	Ka				10.2	
Alcan [37]	Ka	55	55 × 99.5 × 9	791, 792	10.8	44.9
Kymeta [38], [39]	Ku	75	89.5 × 89.5 × 12.3	791, 792	11.25	45.5
XPhased [40], [41]	Ku	75	100 × 60 × 8	791, 792	12	46
	Ka		95 × 62 × 8	791, 792	11	51
*Dimensions corresponding to the antenna alone.						

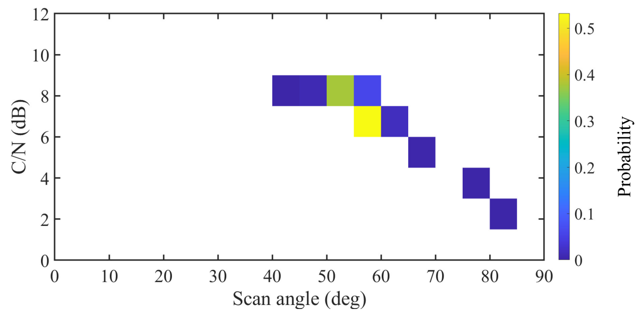

(a)

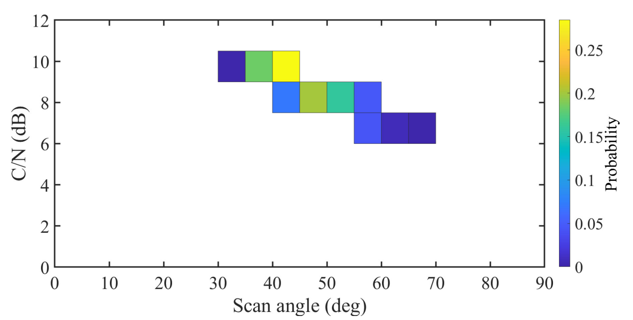

(b)

Fig. 16. GEO access probability at observed scan angle with corresponding C/N for (a) F1 and (b) F2.

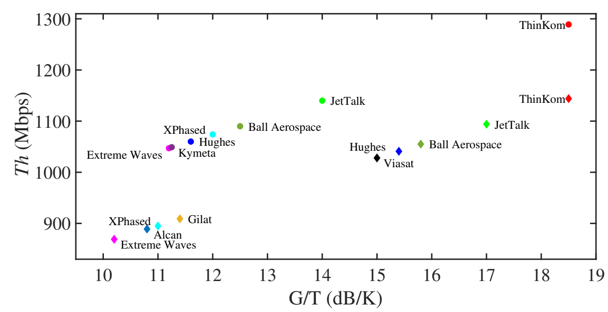

(a) LEO scenario.

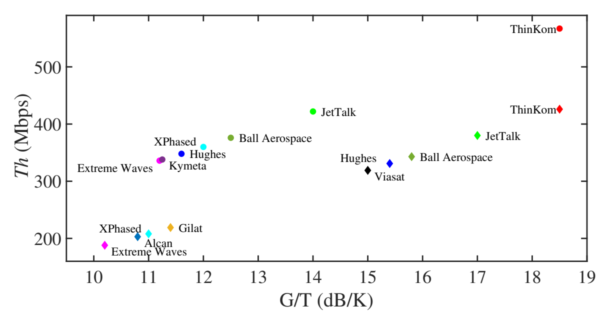

(b) GEO scenario.

Fig. 17. Estimated throughput for commercial terminals.

information about technology aspects is currently available, and hence will not be addressed in this paper.

The theoretical link budget calculations in Sec. IV. were based on the available aperture size. However, the calculations for DL were repeated in this section to determine the throughput using the G/T values of each commercial terminal listed in Table VI. The resulting values are plotted in Fig. 17. Values corresponding to Ku band are indicated by circle-shaped markers, whereas the values corresponding to Ka band are represented by diamond-shaped markers. Except for the G/T values, all assumptions are the same as in the preceding section. As a result, it can be said that the commercial terminals with their advertised G/T value can achieve the resulting throughput in Fig. 17 under the assumed conditions in Sec. IV. It can also be seen that the terminals with a higher G/T value are capable of achieving a higher throughput. The actual throughput obtained with these terminals will differ from the predicted figures because the computations are based on ideal atmospheric conditions and the author's scenario assumptions. However, the gathered data can be used to explain a general trend of the terminal's performance.

VI. Conclusion

Various features of a customer/user terminal antenna unique for avionics satellite communication applications were addressed in this paper. In addition, a link budget analysis was carried out to better understand the achievable link performance for NGSO and GSO scenarios. Finally, utilizing the previously performed link budget analysis, a comparison of the various commercial terminals was performed using their known technical information, which helped in estimating the achievable performance under specified assumptions. This analysis helps in a better understanding of the potential of current technologies for future avionic satellite connectivity.

Acknowledgement

The authors would like to thank the colleagues from Safran Passenger Innovations Germany GmbH for their contributions and for being an inspiration for this paper.

Appendix

details on Link Budget calculation

The link budget calculations were performed based on a square aperture antenna with a maximum dimension (along its diagonal) of 106.68 cm possible using the ARINC 792 [12] footprint. Even though the OAE interface can support at least 1000 W power separately to the transmit and receive aperture, it is additionally stated in [12] that the antenna supplier must define the power supplied to the OAE. Since no particular value is mentioned, a power of 20 W [20] from ThinKom's Ka1717 terminal (which is reported to be ARINC 792 compliant in [20]) was used as reference. The system temperature was calculated with the method followed in [19] using the antenna temperature as 200 K (extracted from sky temperature statistics in [5]) and the LNA noise figure as 1 dB (typical value mentioned in [5]). The terminal's aperture efficiency was taken as 75%, which is the upper bound of the usual range for earth stations as mentioned in [5]. Furthermore, the antenna was assumed to have an ideal cosine roll-off value of 1. Reference values for EIRP and G/T for LEO and GEO satellites were taken from the Starlink constellation [22] and Eutelsat 7B [21] satellite, respectively. Furthermore, a frequency of 17.7 GHz (DL) and 27.5 GHz (UL) was set, considering the lowest edge of the appropriate frequency band (Ka). The FoM of the satellite communication link were computed using the DL and UL carrier bandwidths of 100 MHz and 50 MHz (taken from [43]), respectively.

References

[1] A. P. T. Adithyababu, F. Boulos, and S. Caizzone, "Analysis of user terminal trade-offs for future satellite communication applications," in *27th Ka and Broadband Communications Conference*, Stresa, Italy, 18-21 Oct. 2022.

[2] O. Kodheli, A. Guidotti, and A. Vanelli-Coralli, "Integration of satellites in 5g through leo constellations," in *IEEE Global Communications Conference*, Dec. 2017.

[3] *3rd Generation Partnership Project; Technical specification group radio access network; Solutions for NR to Support Non-Terrestrial Networks (NTN) (Release 16),* 3GPP TR 38.821 V16.1.0, May. 2021.

[4] *3rd Generation Partnership Project; Technical specification group services and system aspects; Study on Using Satellite Access in 5G; Stage 1 (Release 16),* 3GPP TR 22.822 V16.0.0, Jun. 2018.

[5] G. Maral and M. Bousquet, *Satellite Communications Systems: Systems, Techniques and Technology*, 3rd ed. Chichester, UK: Wiley, 1998.

[6] *Systems Tool Kit (STK) 12.5.0*, Analytical Graphics, Inc.

[7] *Satellite Earth Stations and Systems (SES); Satellite mobile Aircraft Earth Stations (AESs) operating in the 11/12/14 GHz frequency bands; Harmonised Standard for access to radio spectrum,* ETSI EN 302 186 V2.2.1, 2021.

[8] *Satellite Earth Stations and Systems (SES); Harmonised Standard for Earth Stations on Mobile Platforms(ESOMP) transmitting towards satellites in non-geostationaryorbit, operating in the 27,5 GHz to 29,1 GHz and 29,5 GHz to 30,0 GHz frequency bands covering the essentialrequirements of article 3.2 of the Directive 2014/53/EU,* ETSI EN 303 979 V2.1.1, 2016.

[9] J. Christensen, "ITU Regulations for Ka-band Satellite Networks," Sep. 2012. [Online]. Available: https://www.itu.int/dms_pub/itu-r/md/12/iturka.band/c/R12-ITURKA.BAND-C-0001%21%21PDF-E.pdf

[10] *Mark I Aviation Ku-band and Ka-band satellite communication system: Part 1: Physical installation and aircraft interfaces,* ARINC Characteristic 791P1-3, Sep. 2019.

[11] *Mark I Aviation Ku-band and Ka-band satellite communication system: Part 2: Electrical interfaces,* ARINC Characteristic 791, Jul. 2013.

[12] *Second generation Ku- band and Ka-band satellite communication system,* ARINC Characteristic 792, Dec. 2018.

[13] "FlightGear™ ARINC 791 Ka, Ku, Ka/Ku Universal Installation datasheet." [Online]. Available: https://www.carlisleit.com/wp-content/pdfs/prodinfo/SS-10025%20FlightGear%20ARINC%20791.pdf

[14] "FlightGear™ ARINC 792 Ka, Ku, Ka/Ku Universal Installation datasheet." [Online]. Available: https://www.carlisleit.com/wp-content/pdfs/prodinfo/SS-10100%20FlightGear%20ARINC%20792.pdf

[15] *Earth station antenna performance standards*. [Online]. Available: https://www.ecfr.gov/current/title-47/chapter-I/subchapter-B/part-25/subpart-C/section-25.209

[16] *Off-axis EIRP density envelopes for FSS earth stations transmitting in certain frequency bands*. [Online]. Available: https://www.ecfr.gov/current/title-47/chapter-I/subchapter-B/part-25/subpart-C/section-25.218

[17] "FlightGear™ ARINC 791 Ka, Ku, Ka/Ku Universal Installation." [Online]. Available: https://www.carlisleit.com/markets/commercial-aerospace/ifeci/connectivity-kits/arinc-791-universal-installation-solutions/

[18] W. L. Stutzman and G. A. Thiele, "Array antennas," in *Antenna Theory and Design*, 3rd ed. Hoboken, USA: Wiley, 2012.

[19] "Link budget calculations for a satellite link with an electronically steerable antenna terminal," Jun. 2019. [Online]. Available: https://www.kymetacorp.com/wp-content/uploads/2020/09/Link-Budget-Calculations-2.pdf

[20] "Thinkom ThinAir Ka1717 Datasheet." [Online]. Available: https://www.thinkom.com/wp-content/uploads/2022/06/thinair-ka1717-datasheet.pdf

[21] "Eutelsat 7B." [Online]. Available: https://www.eutelsat.com/files/PDF/brochures/EUTELSAT_SATELLITE_E7B.pdf

[22] A. Aguilar, P. Butler, J. Collins, M. Guerster, B. Kristinsson, P. Mckeen, K. Cahoy, and E. Crawley, "Tradespace exploration of the next generation communication satellites," 07-11 Jan. 2019.

[23] *Real-time Worldwide Flight Traffic*. [Online]. Available: https://flightaware.com/

[24] *Jonathan's Space Pages: Starlink Statistics*, 04 Dec. 2022. [Online]. Available: https://planet4589.org/space/con/star/stats.html

[25] "The axes of flight." [Online]. Available: https://www.nasa.gov/sites/default/files/atoms/files/the_axes_of_flight.pdf

[26] "A380-800 flight deck and systems briefing for pilots." [Online]. Available: https://idoc.pub/documents/a380-800-flight-deck-systems-briefing-for-pilots-546gzx5ey7n8
[27] "A350-900 flight deck and systems briefing for pilots." [Online]. Available: https://doku.pub/documents/a350-900-flight-deck-and-systems-briefing-for-pilots-1pdf-el9vpwjekjqy
[28] "Thinkom ThinAir Ku3030 Datasheet." [Online]. Available: https://www.thinkom.com/wp-content/uploads/2022/03/thinair-ku3030-datasheet_thinkom.pdf
[29] "Thinkom ThinAir Ka2517 Datasheet." [Online]. Available: https://www.thinkom.com/wp-content/uploads/2022/03/thinair-ka2517-datasheet.pdf
[30] M. C. Viganó, "Ka band phased array developments at ViaSat," presented at 16th European Conference on Antennas and Propagation (EuCAP 2022), Madrid, Spain, 27 Mar.-01 Apr. 2022.
[31] "Ball Aerospace Ku Terminal." [Online]. Available: https://www.ball.com/getattachment/07a0fcd9-df91-4464-8326-1780a1acd7ac/D3285_Ku-SATCOM_Brochure_Updated_20210819.pdf
[32] "Ball Aerospace Ka Terminal." [Online]. Available: https://www.ball.com/getattachment/157cc0d7-ddc3-4458-b787-553d74cc5ef4/D3285_Ka-SATCOM_Brochure_Updated_20210819.pdf
[33] "JetTalk." [Online]. Available: https://jet-talk.com/wp-content/uploads/2019/05/14351_Jet_Talk_Brochure_i-print.pdf
[34] "Hughes Aero." [Online]. Available: https://www.hughes.com/sites/hughes.com/files/2021-12/H59116-Hughes_Aero-DS.pdf
[35] G. Expósito-Domínguez, F. J. Jiménez, A. Gal, A. Volodarsky, and B. Marinov, "Flight test campaign of Embedded Electronically Steerable SATCOM Aero Antenna for Clean Sky 2 project," in *2022 16th European Conference on Antennas and Propagation (EuCAP)*, Madrid, Spain, 27 Mar.-01 Apr. 2022.
[36] "Extreme Waves." [Online]. Available: https://www.extreme-waves.com/satcom
[37] "ALCAN Datasheet." [Online]. Available: https://www.alcansystems.com/files/data-sheets/2020-06-15_Data-Sheet-Antenna.pdf
[38] "Kymeta u8 Terminal Datasheet," Accessed: May, 2022. [Online]. Available: https://www.kymetacorp.com/wp-content/uploads/2021/12/700-00071-000-revJ-Kymeta-u8-antenna-product-sheet.pdf
[39] "Kymeta u8 Terminal Datasheet," Accessed: May, 2022. [Online]. Available: https://www.kymetacorp.com/wp-content/uploads/2021/12/700-00097-000-revJ-Kymeta-u8-terminal-product-sheet.pdf
[40] "XPhased Ku Terminal." [Online]. Available: http://www.xphased.com/Products/x-aesa/1.html
[41] "XPhased Ka Terminal." [Online]. Available: http://www.xphased.com/Products/x-aesa/2.html
[42] F. Boulos, K. Yinusa, U. Johannsen, and S. Caizzone, "Array antenna as ground terminal for internet everywhere by satellite: A review," *Proc. IEEE*, 2022 (submitted).
[43] "Request for experimental authorization," 01 Nov. 2021. [Online]. Available: https://apps.fcc.gov/els/GetAtt.html?id=285359&x=

Aparna P. T. Adithyababu received the B.Tech degree in Electronics and Communication Engineering from Amrita School of Engineering, Kerala, India, in 2017 and M.Sc degree in Communications Engineering from the University of Applied Sciences, Darmstadt, Germany, in 2021. As a recipient of DAAD scholarship, she is presently a member of the Antenna Systems Group at the Institute of Communications and Navigation of the German Aerospace Center (DLR), where she is working on her doctoral studies on steerable high-performance antenna systems for global connectivity.

Federico Boulos received the BSc degree in telecommunications and electronics engineering and the MSc in information and communications engineering from the University of Trento, Trento, Italy. He is currently a member of the Antenna Systems Group at the Institute of Communications and Navigation of the German Aerospace Center (DLR), where he is responsible for development of innovative antennas for satellite communications. Moreover he is currently pursuing the Ph.D. with the Electromagnetics group at the TU/e department of Electrical Engineering.

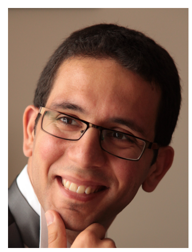

Stefano Caizzone received the M.Sc. in Telecommunications Engineering and the Ph.D. degree in Geoinformation from the University of Rome "Tor Vergata", Italy, in 2009 and 2015, respectively. Since 2010, he is with the Antenna group of the German Aerospace Center (DLR), where he has been responsible for the development of innovative miniaturized antennas. Since July 2020, he leads the Antenna Systems Group. His main research interests concern small antennas for satellite navigation, controlled radiation pattern antennas for robust satellite navigation and high-performance antenna design for precise satellite navigation, antenna arrays for satellite communication and installed performance analysis.